



Article

The Effect of Air leakage through the Air Cavities of Building Walls on Mold Growth Risks

Yonghui Li ^{1,2}, Xinyuan Dang ¹, Changchang Xia ¹, Yan Ma ¹, Daisuke Ogura ³ and Shuichi Hokoi ^{1,*}

¹ School of Architecture, Southeast University, #2 Sipailou, Xuanwu District, Nanjing 210096, Jiangsu Province, China; liyonghui@seu.edu.cn (Y.L.); dangxinyuan@seu.edu.cn (X.D.); xia_2017@seu.edu.cn (C.X.); mayan0925@seu.edu.cn (Y.M.)

² Key Laboratory of Urban and Architectural Heritage Conservation of Ministry of Education (Southeast University), #2 Sipailou, Xuanwu District, Nanjing 210096, Jiangsu Province, China

³ Department of Architecture and Architectural Engineering, Kyoto University, Kyotodaigaku-Katsura, Nishikyo-ku, Kyoto 6158540, Japan; ogurad@archi.kyoto-u.ac.jp

* Correspondence: hokoi@seu.edu.cn; Tel.: +86-025-83790530

Received: 28 January 2020; Accepted: 29 February 2020; Published: 4 March 2020



Abstract: Mold growth poses a high risk to a large number of existing buildings and their users. Air leakage through the air cavities of the building walls, herein gaps between walls and air conditioner pipes penetrating the walls, may increase the risks of interstitial condensation, mold growth and other moisture-related problems. In order to quantify the mold growth risks due to air leakage through air cavity, an office room in a historical masonry building in Nanjing, China, was selected, and its indoor environment has been studied. Fungi colonization can be seen on the surface of air conditioner pipes in the interior side near air cavity of the wall. Hygrothermometers and thermocouples logged interior and exterior temperature and relative humidity from June 2018 to January 2020. The measured data show that in summer the outdoor humidity remained much higher than that of the room, while the temperature near the air cavity stays lower than those of the other parts in the room. Hot and humid outdoor air may condense on the cold wall surface near an air cavity. A two-dimensional hygrothermal simulation was made. Air leakage through the air cavities of walls proved to be a crucial factor for mold growth.

Keywords: building walls; air cavity; summer condensation; mold growth risks; air-conditioner

1. Introduction

Dampness and mold growth are commonly observed in residences, offices and other buildings [1], resulting in economic [2] and environmental [3] problems. World Health Organization's guidelines [4] even emphasized that the priority of maintaining indoor air quality is to minimize persistent dampness and microbial growth on interior surfaces and in building structures. Accumulation and dispersion of fungi spores, cell fragments, allergens, and microbial volatile organic compounds (MVOCs) lead to severe human health hazards [5]. Specifically, indoor mold will increase the risk of chronic rhinosinusitis hypersensitivity, pneumonitis/allergic alveolitis and allergic fungal sinusitis [6–9]. Chronical exposures to microbial contaminants can trigger sick building syndrome (SBS) [10–12], including asthma, rhinitis or bronchitis symptoms.

The occurrence of mold growth is mainly caused by a favorable hygrothermal environment: appropriate temperature; high relative humidity; and sufficient substrate and exposure time [1,13]. Among these factors, nutritional requirements seem to be minimal and could be easily satisfied either by the building materials or by dust or other deposits [14,15], while the amount of water available on/in

wall materials is the most important factor triggering the growth of microorganisms. The United States (US) Center for Disease Control stated in its guidance that “elimination of moisture intrusion and leaks and removal of mold” constitutes one of the three crucial interventions for houses implementation [16].

Currently, advanced mold prediction models deal with the main influencing factors for mold growth: the surface temperature and relative humidity. Vereecken et al. [17] reviewed the models for mold growth and environmental risk prediction (isopleth systems [18,19], bio-hygrothermal model [20], ESP-r mold prediction model [21,22], VTT model [23]). Abe et al. [24] developed the fungal index to indicate the environmental capacity for mold growth. Hukka et al. [25] proposed a quantitative relationship between mold growth initiation conditions, maximum growth and growth rate. Sedlbauer [26] developed WUFI-Bio software (Klaus Sedlbauer, Department Hygrothermics at the Fraunhofer IBP, Munich, Germany) to assess mold risk by temperature, humidity and substrate in cases of transient conditions. Heat and moisture transfer simulation coupled with suitable temperature and humidity conditions for mold growth can also be used for evaluation [27].

Building walls made of porous bricks or stones are easily exposed to outdoor moisture, including wind-driven rain [28] and rising dampness [29]. Additionally, improper energy conservation treatment [30–32], including inadequate insulation and unwanted air pathways, may cause thermal bridges and allow the surface temperature to become lower than the dew point of surrounding air, leading to unwanted condensation. Among them, air leakage through an air cavity [33] serves as one of the main moisture-transferring routes, redistributing the temperature and humidity of walls.

In addition to scaling, crumbling, cracking and other natural mechanical damage, improper handling of building facades also generates air cavities through walls. The commonest case is air conditioner pipes or electrical wires that penetrate the walls with poor sealing; even though the air cavity is carefully sealed, the sealing materials will degrade with time (Figure 1).

An air cavity, as a main route for air leakage, increases the energy consumption and causes moisture-related problems. It is even worse when the cooling system is operated in summer [34,35]. Hot and humid air is cooled down and even condenses when passing over the cold-refrigerant plumbing, drainage pipes of air conditioning units and adjacent cold wall surfaces. The condensed water and accumulating dust [36] around the air cavity are suitable for fungi spores to settle down.

The effects on energy loss [37–39] and air quality [40,41] due to air leakage of buildings have been investigated in many studies. Moisture-related problems because of air leakage through some specific building components, for instance, the attic [42], were also analyzed. However, there is not sufficiently thorough quantitative research for mold growth risks due to air leakage through air cavities of building walls.

This research aims to investigate the existence and possible sources of the dampness and mold growth in a historical office building in Nanjing, China, a typical city that chronically suffers from high humidity during long rainy seasons. The severe smell of mold and a sense of discomfort were frequently experienced in the room we monitored, especially during a sticky summer. Air leakage through the air cavity around the air conditioner pipe hole was suspected to be the major reason for moisture intrusion, condensation and mold growth. The temperature and relative humidity around the hole were monitored by hygrothermometers and thermal couples from June 2018 to January 2020.

A two-dimensional hygrothermal simulation was also conducted, using the measured datasets as boundary conditions, to investigate hygrothermal performance of the wall with air leakage through the air cavity. The measured indoor temperature and relative humidity were used for validation. Mold growth risks, considering the effects of precipitation, solar radiation and the speed of air flow through the air cavity, were estimated.

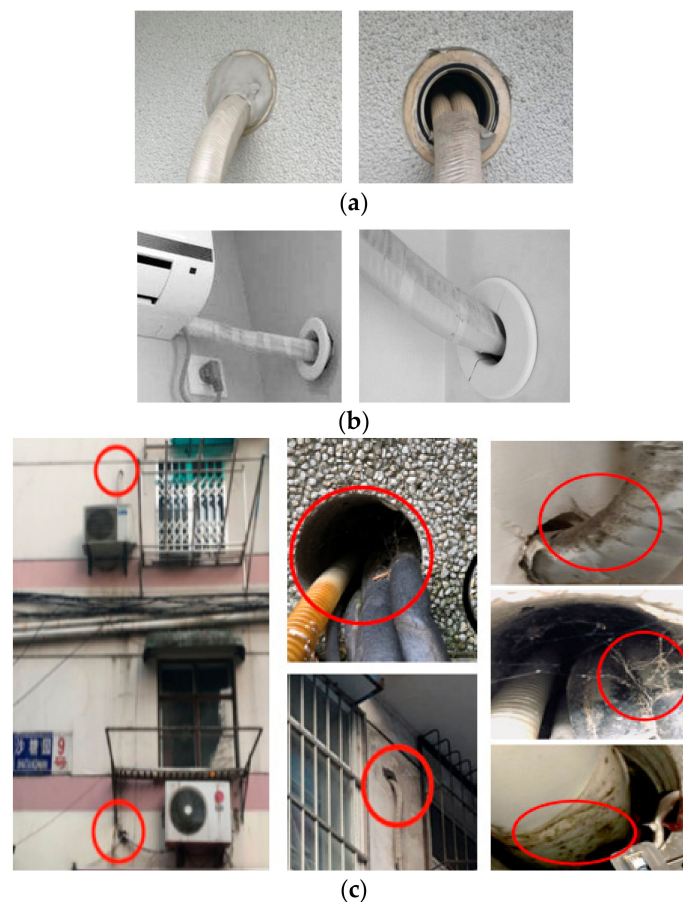


Figure 1. Air cavity through which air conditioner pipes pass: (a) a hole sealed with mud and the case after aging and shedding; (b) a hole through the wall of a newly built dwelling without sealing; (c) air conditioner pipe holes through the wall without sealing are very common in old buildings, and dust and mold accumulate.

2. Experimental Setup

2.1. Survey

The building we monitored was a historical masonry building located in Nanjing, China (Figure 2a). It was constructed in the 1920s and was restored and extended in 1952, 1957, 1988, 1996 and 2011. Now it has three floors with a semi-basement, and the total construction area is 6827 m². This building, with south-north orientations, is still used as an office building and for teaching. Shrubs surround the building and tall *Platanus* shade it from the sun during hot seasons.

The walls were originally blue bricks (240 mm thickness) with concrete and cement mortar surfaces. In the 1980s, the foundation was strengthened and waterproofed, while the terrazzo floor layer was changed into timber-framework floor. Although the interior walls have been repainted by cement mortar, the exterior wall remains untreated to maintain the historical facade. However, these porous building materials are especially vulnerable to rising damp, wind-driven rain and interstitial condensation. Things became even worse when the air conditioner pipe holes penetrated the wall, promoting air leakage through the air cavity. Figure 2b,c shows the air cavity in the corner. It is not carefully sealed, and severe mold colonization can be found on the surface of pipes nearby.

The infrared thermography data in Figure 3 illustrate that the air cavity area was significantly colder than the adjacent areas, which might have resulted from the air leakage through the air cavity. The temperature difference between the hole and adjacent area reached up to 5 °C (indoors) or 20 °C

(outdoors). In cooler seasons, hot and humid outdoor air is cooled down when passing through the cold air cavity, leading to the condensation and mold growth.

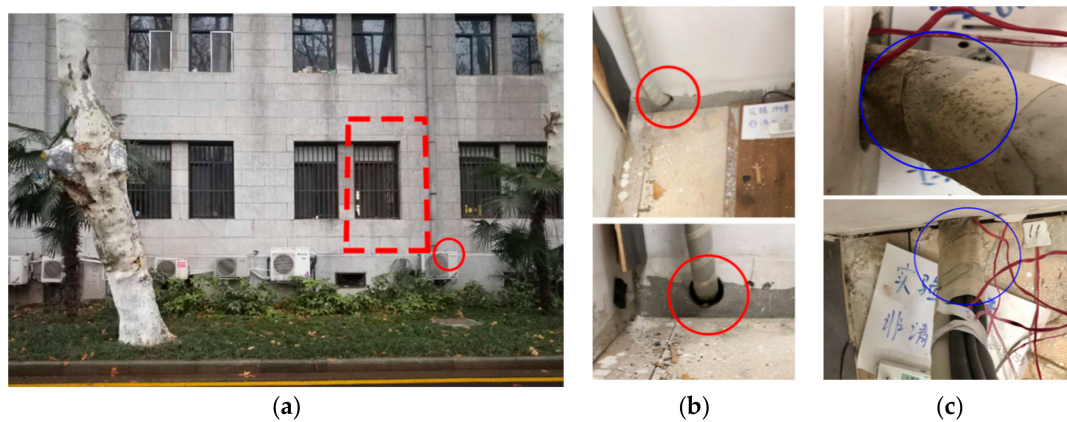


Figure 2. The monitored building and the monitored room: (a) The main facade of the monitored building and the monitored room (in red dashed line) with the air conditioner pipe hole, i.e., the air cavity (in red circle); (b) the air cavity in the monitored room without sealing; (c) mold colonization near the air cavity (in blue circle).

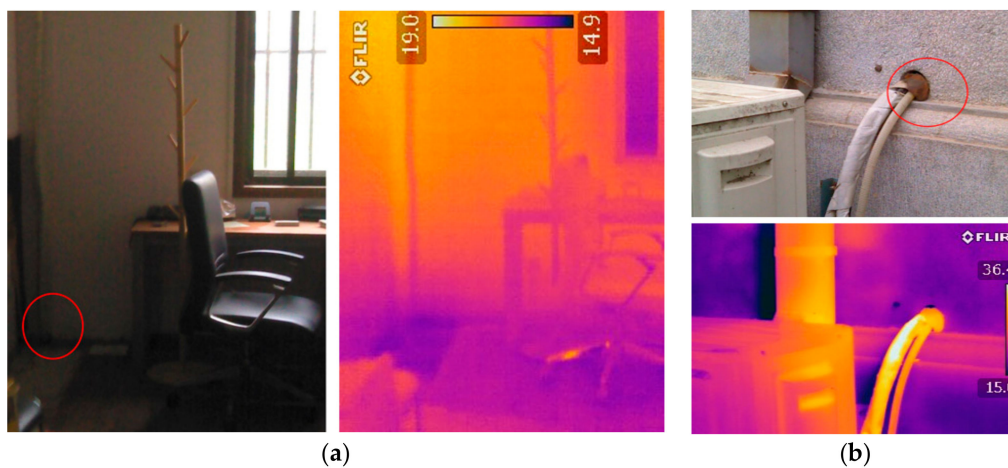


Figure 3. Infrared thermography of the air cavity area (in red circle) viewed from: (a) inside and (b) outside.

2.2. Monitoring

The monitored room (Figure 4) is on the first floor with a window to outside facing south, and it connects to the indoor corridor to the north. It has been used as an office for years. The severe moldy smell and dampness were experienced during hot and rainy days.

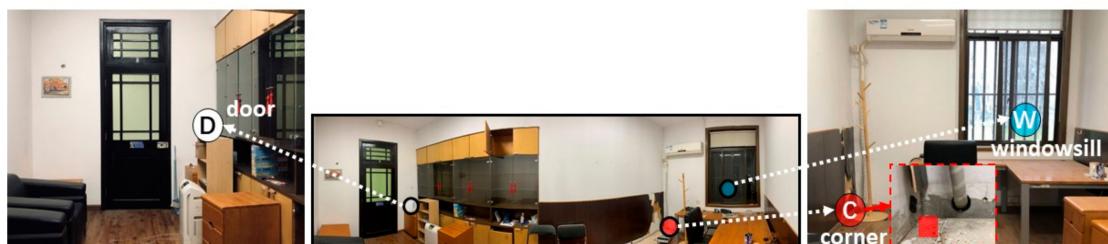


Figure 4. Indoor panorama of the monitored room, with three hygrothermometers monitoring the air temperature and relative humidity.

The monitoring lasted for one and a half years, from June 2018 to January 2020. The door and window were closed except for limited periods when researchers (some of the authors) entered the room to read the data. In order to eliminate the thermal influence of the air conditioner, the room was not cooled by the air conditioner in the summer of 2018, while in the summer of 2019, the cooling system was operated for several days for comparison.

Nine hygrothermometers (HOBO data loggers) were placed in the monitored room (3 sensors, as shown in Figure 4), corridor (1 sensor), next rooms (4 sensors) and outdoor area (1 sensor). They recorded air temperature and relative humidity every 30 minutes. Six sets of thermocouples (shown in Figure 5) were placed around the air cavity to record the surface temperature every 30 minutes. Tables 1 and 2 list their positions and purposes.

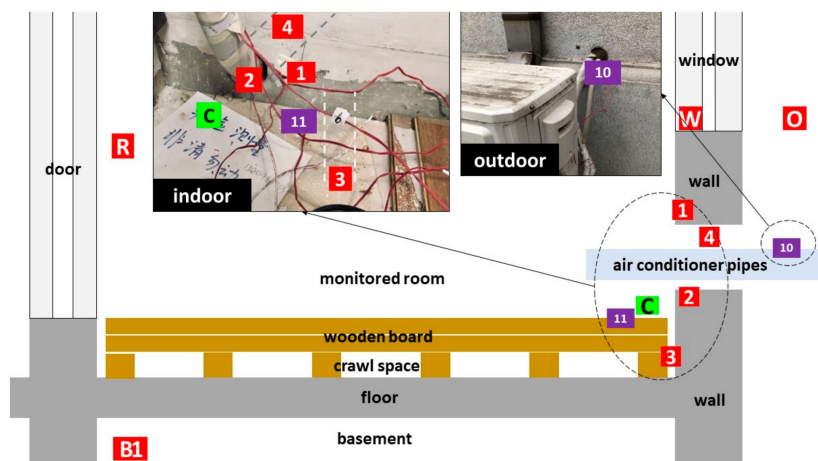


Figure 5. The thermocouples in the monitored room measuring the surface temperature.

Table 1. Positions and purposes of hygrothermometers.

NO.	Position	Purposes
#D	Monitored room—Door	Validation
#C	Monitored room—Corner, near the air cavity	Comparison
#W	Monitored room—Windowsill	Comparison
#O	Outdoors	Boundary conditions
#1C	Corridor	Boundary conditions
#B1	Basement	Boundary conditions
#2F	Next room on the second floor	Boundary conditions
#1L	Next room on the left (on the first floor)	Comparison
#1R	Next room on the right (on the first floor)	Comparison

Table 2. Positions of thermocouples.

NO.	Position
#1	On the wall surface near the hole
#2	About 1cm deep inside the hole, on the lower surface
#3	About 20 cm deep under floorboard and in the gap between wall surface and floor board/crawl space
#4	About 15 cm deep in the air cavity between pipes and upper surface (not contact with the wall)
#10	On the surface of drainage pipe (outdoor)
#11	On the surface of floor board

Moisture meters (Testo North America, West Chester, PA 19382, United States) were used to measure the surface water content of the wall surface on several days in the summer of 2019. Figure 6 shows their positions.

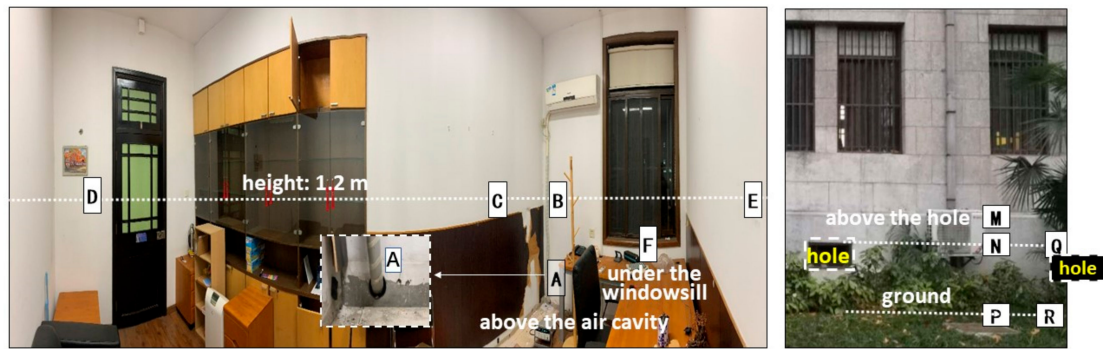


Figure 6. Surface water content measuring points (July and August 2019).

3. Simulation

3.1. Governing Equations

In this research, we developed a Fortran simulation code based on Matsumoto's hygrothermal transient and simultaneous transfer equations (Equations (1)–(7)) [43]. The finite difference method (central difference) and time forward scheme [44] were adopted. In the heat and moisture balance of the air in the cavity, the upwind scheme was used for stability.

The model was based on the following assumptions: the material is an isotropic, non-deformable, solid, porous medium that does not chemically react with water; water in different phases (only liquid and gas phases) is in an equilibrium state inside the material; the difference in the moisture absorption and desorption processes of the material is neglected (no hysteresis).

The migration of heat and moisture in a porous material, brick in this paper, is a thermophysical phenomenon in which the water changes phases, producing latent heat, accompanied by changes in water content. In this paper, water's chemical potential (Gibb's free energy) was used as the moisture potential on the basis of nonequilibrium thermodynamics:

$$\mu = R_v T \ln(RH) \quad (1)$$

where μ (J/kg) is the water chemical potential; T (K) and RH (%) are the absolute temperature and relative humidity, respectively; R_v is the gas constant of water vapor ($R_v = R/M_v$); R is the general gas constant; and M_v is the water vapor molecular weight.

The basic equations for heat and moisture balance are given by Equations (2) and (3):

$$c\rho \frac{\partial T}{\partial t} = -\nabla \cdot q_s + r\nabla \cdot j_{1w} \quad (2)$$

$$\rho_w \frac{\partial \psi}{\partial \mu} \frac{\partial \mu}{\partial t} = -\nabla \cdot (j_{1w} + j_{2w}) \quad (3)$$

where $c\rho$ [J/(m³·K)] is the heat capacity of material, q_s (J/(s·m²)) is the heat flux, r [J/kg] is the latent heat of phase change from gas to liquid phase, ρ_w (kg/m³) is the density of water, ψ [m³/m³] is the volumetric water content and j_{1w} and j_{2w} (kg/(s·m²)) are the water fluxes in gas and liquid phases, respectively:

$$J_{1w} = -\lambda'_{\mu g} (\nabla \mu - n_x g) - \lambda'_{Tg} \nabla T \quad (4)$$

$$J_{2w} = -\lambda'_{\mu l} (\nabla \mu - n_x g) - \lambda'_{Tl} \nabla T \quad (5)$$

The two-dimensional hygrothermal model was used in the simulation, and heat and moisture balance equations inside the material are given by Equations (6) and (7):

$$c\rho \frac{\partial T}{\partial t} = \frac{\partial}{\partial x} \left[(\lambda + r\lambda'_{Tg}) \frac{\partial T}{\partial x} + r\lambda'_{\mu g} \left(\frac{\partial \mu}{\partial x} - n_x g \right) \right] + \frac{\partial}{\partial y} \left[(\lambda + r\lambda'_{Tg}) \frac{\partial T}{\partial y} + r\lambda'_{\mu g} \left(\frac{\partial \mu}{\partial y} - n_y g \right) \right] \quad (6)$$

$$\rho \omega \frac{\partial \psi}{\partial \mu} \frac{\partial \mu}{\partial t} = \frac{\partial}{\partial x} \left[\lambda'_{\mu} \left(\frac{\partial \mu}{\partial x} - n_x g \right) + \lambda'_{T} \frac{\partial T}{\partial x} \right] + \frac{\partial}{\partial y} \left[\lambda'_{\mu} \left(\frac{\partial \mu}{\partial y} - n_y g \right) + \lambda'_{T} \frac{\partial T}{\partial y} \right] \quad (7)$$

The air temperature and humidity of the monitored room were expressed based on one volume (mass) of room air using the concept of a simplified zonal model. The heat and moisture (vapor) fluxes from the wall and floor surfaces were calculated by a two-dimensional model. After being multiplied by the related surfaces, they were used in the three-dimensional energy and moisture balance equations of the room air, whose air balance was calculated using a zonal simplified model. The following Equations (8) and (9) are used to calculate the temperature and humidity of the room air. Three terms on the right hand represent the sum of heat or moisture fluxes on the surfaces, heat or moisture transfer due to the air flow through the window and heat or moisture transfer due to air leakage through the air cavity, respectively.

Heat balance of the room air:

$$c\rho V_{rm} \frac{dT}{dt} = \sum Q_s + c\rho V_{rm} \cdot n \cdot (T_{out} - T_{in}) + c\rho V_{cv} \cdot (T_{out} - T_{in}) \quad (8)$$

Moisture balance of the room air:

$$\rho V_{rm} \frac{d(AH)}{dt} = \sum J_s + \rho V_{rm} \cdot n \cdot (AH_{out} - AH_{in}) + \rho V_{cv} \cdot (AH_{out} - AH_{in}) \quad (9)$$

where $c\rho$ [J/(m³·K)] is the heat capacity of material; V_{rm} [m³] is the volume of the room (for the two-dimensional model, the length on Z-axis equals 1); S_{cv} [m²] is the sectional area of the air cavity; v [m/s] is the air flow velocity through the air cavity (X-axis); n [1/s] is the ventilation rate of the room (air flow through the window); $\sum Q_s$ [J/s] and $\sum J_s$ [kg/s] are the sums of heat and moisture fluxes on the wall surfaces, respectively; T_{out} and T_{in} [K] are the temperatures of the outdoor and the room air, respectively; AH_{out} and AH_{in} [kg/kg] are the absolute humidities of the outdoor and the room air, respectively.

3.2. Simulated Room and Wall Structure

Simplified from the main section of the monitored room, a two-dimensional hygrothermal simulation model was made, as shown in Figure 7a. The size of the room was 4 m in depth and 3 m in height, with a door (2 m) and a window (1 m), and the thickness of floors and walls was 200 mm. The characteristics of the typical brick in South China were used as the material properties [45] for the walls and floors in the simulation. As Figure 7b shows, pipe cells (located at $x = 10.2\text{--}10.4$ m, $y = 16.25\text{--}16.30$ m) that make contact with the lower surface of the air cavity and air cells (located at $x = 10.2\text{--}10.4$ m, $y = 16.30\text{--}16.35$ m) are set in the air cavity area. Heat conduction occurs between the pipe cells and lower cavity surface, while convective transfer between the upper surface of the cavity and air flow happens through air cells. Pipe cells were given smaller heat capacities and larger thermal resistance values compared with wall cells, and they are assumed as impermeable to moisture.

The measured temperatures and relative humidity in the corridor (#C), outdoors (#O), basement (#B1) and second floor (#2F) were used as boundary conditions. The heat and moisture balance of the air in the air cavity were dealt with assuming one-dimensional air flow with a velocity v (m/s). Ventilation rate of the air flow through the door and the window was given a fixed value (1.0/hour), since the door and the window remained closed during the monitoring. The solar radiation was given a reduction coefficient (0.5) considering the shading effects of the trees. Physical parameters [46] used in the simulation are shown in Table 3.

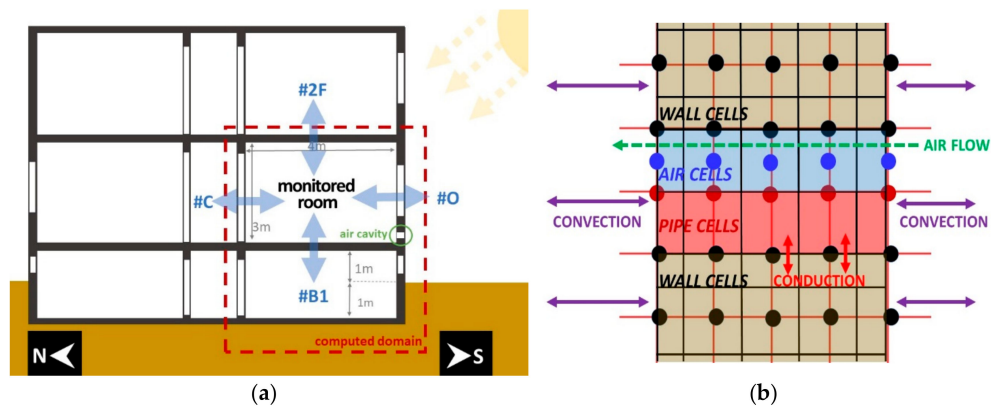


Figure 7. Simulated model: (a) computed domain; (b) pipe and air cells.

Table 3. Physical parameters.

Item	Value (unit)
Indoor combined (convection + radiative) heat transfer coefficient (α_{in})	$10 \left(\frac{W}{m^2 \cdot K} \right)$
Outdoor combined (convection + radiative) heat transfer coefficient (α_{out})	$18 \left(\frac{W}{m^2 \cdot K} \right)$
Moisture transfer coefficient (α')	$1.1 \times 10^{-7} \left(\frac{kg}{m^2 \cdot s} \right)$
Heat capacity of the air ($c\gamma$)	1255.8 (J/K)
Moisture capacity of brick ($c\gamma'$)	$7.5 \times 10^{-6} \left(\frac{kg}{m^3 \cdot Pa} \right)$

4. Measurement Results and Discussion

4.1. Weather Conditions

Nanjing is a subtropical city, in which the monitored building is located. Its temperature ranges from -13.1 °C to 39.7 °C, with the average at 15.4 °C. It has abundant rainfall (annual average rainfall at 1106.5 mm) and a high humidity level (annual average relative humidity at 76%), especially for the rainy season from late June to early July. Figures 8 and 9 show temperature with relative humidity, and the solar radiation with the rainfall from June 2018 to June 2019, respectively.

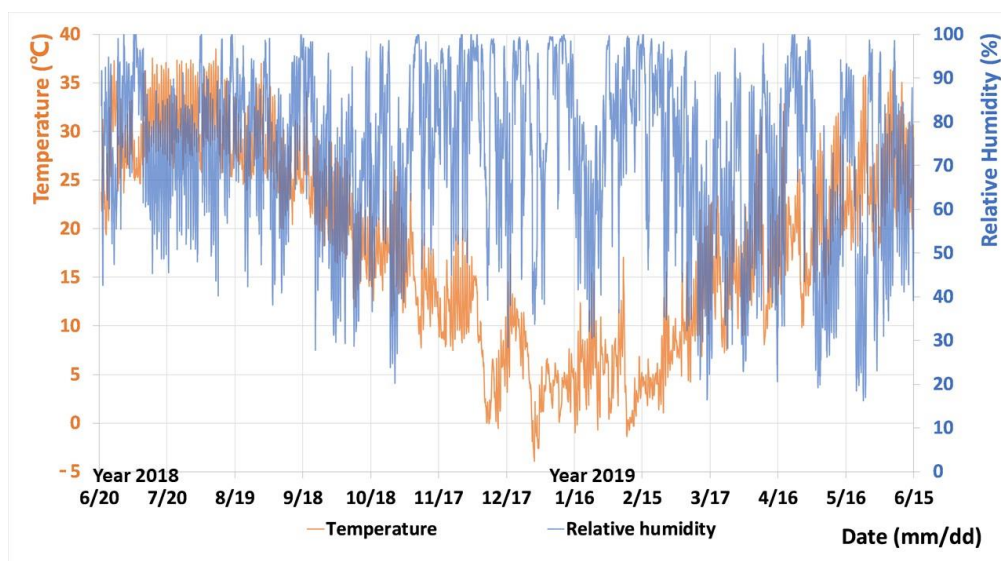


Figure 8. Temperature and relative humidity of Nanjing from June 2018 to June 2019, (source: weather station in Southeast University, Nanjing, China).

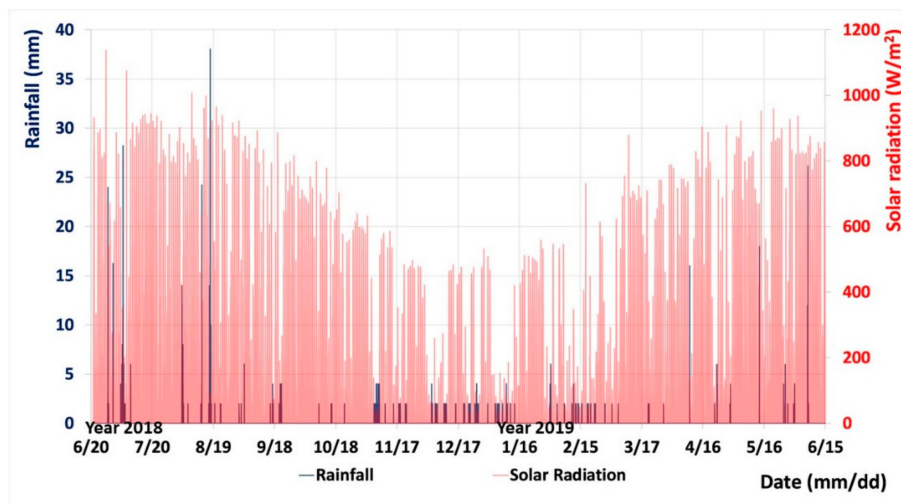


Figure 9. Solar radiation and rainfall of Nanjing from June 2018 to June 2019, (source: weather station in Southeast University, Nanjing, China).

4.2. Next Rooms and the Outdoors

The measured temperature and relative humidity in the next rooms (#C/corridor, #O/outdoor, #2F/second floor, #B1/basement) are shown in Figure 10. They were used as the input boundary conditions in the simulation. The outdoor temperature changed from $-3\text{ }^{\circ}\text{C}$ to $37\text{ }^{\circ}\text{C}$ throughout the year, with which that of the corridor and basement shared a similar trend. In winter, the temperature difference between the outdoors and the corridor amounted to $10\text{ }^{\circ}\text{C}$, while in summer, the basement temperature remained the lowest, even $10\text{ }^{\circ}\text{C}$ lower than the outdoor temperature. The room on the second floor is an office in use, and the temperature was controlled by the air conditioner in winter (late November–early April) and summer (late June–early September).

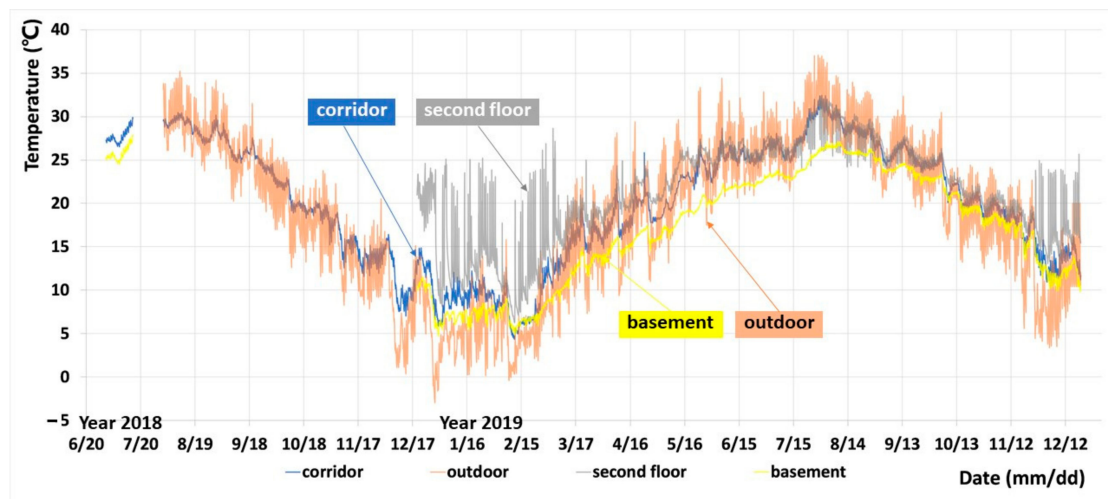


Figure 10. The measured temperature of the next rooms and the outdoors.

As shown in Figure 11, the outdoor relative humidity experienced sharp peaks and troughs throughout the year and stayed over 90% during nights in the summer and winter. It must be noted that the basement relative humidity surged roughly up to 100% for considerable times. At two time zones, from 4 a.m. to 6 a.m. and from 7 p.m. to 9 p.m., both the outdoor and basement humidity was very high. Although the corridor's relative humidity was from 50% to 60% for a relatively long period, it remained at 70–90% from late June to early September. The relative humidity on the second floor decreased to 22% due to the heating operation of the air conditioner, which may cause discomfort.

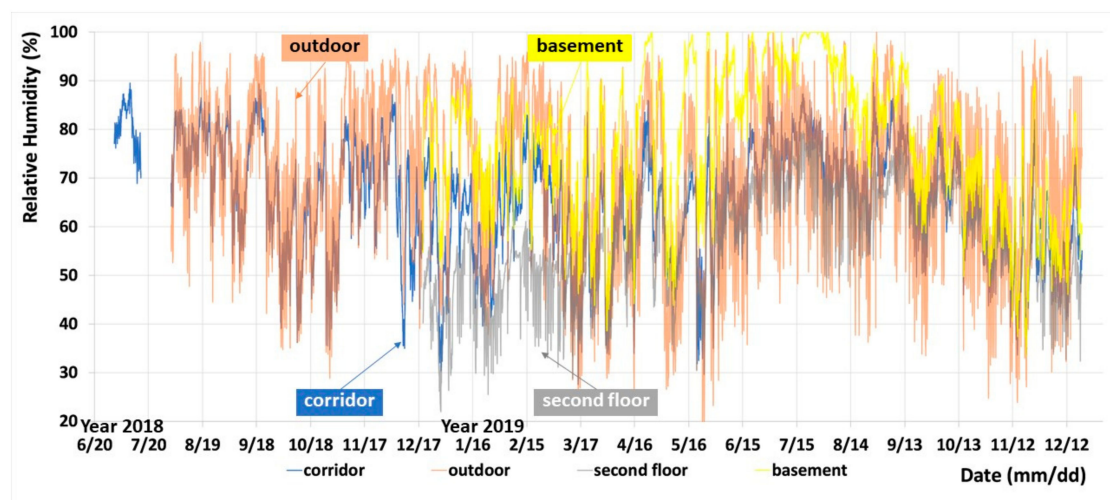


Figure 11. The measured relative humidity of the next rooms and the outdoors.

4.3. Comparison among the Rooms

The indoor conditions of the monitored room and the three office rooms in use (#1R/right neighboring room, #1L/left neighboring room, #2F/second floor) were compared as follows.

As shown in Figure 12, the air temperatures in the left, right, and second floor rooms were maintained at around 20–25 °C both in the summer and winter by the air conditioners, and the diurnal temperature difference was 10 °C in the summer and 15 °C in the winter. In the summer, the room temperature on the second floor was by 2–5 °C higher than in the rooms on the first floor, even with cooling.

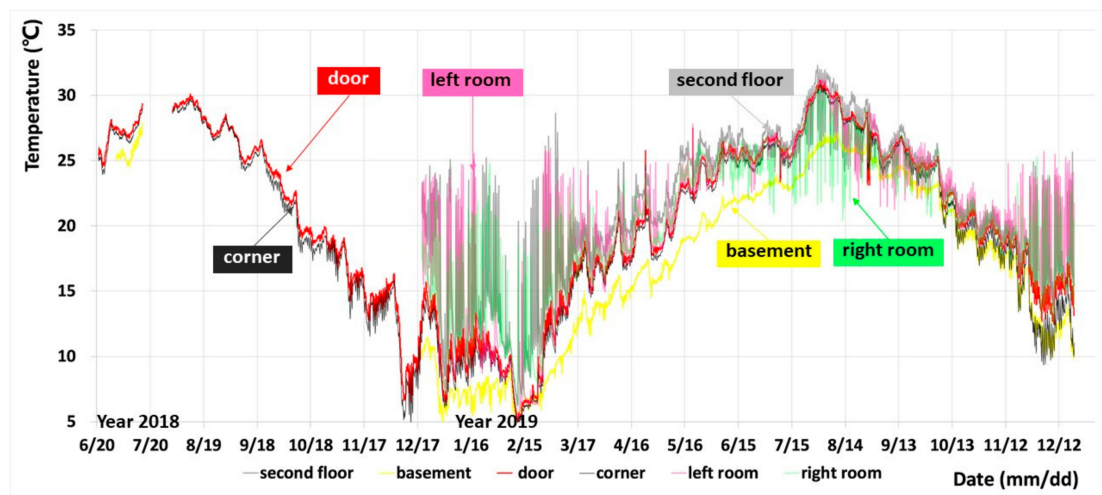


Figure 12. The measured temperatures of the office rooms.

Figure 13 shows that the relative humidity in the monitored room was almost always higher than in other rooms. The relative humidity near the corner (near the air cavity) was higher than that near the door, especially from August to early October, which might have been caused by the moisture supply from the exterior environment through the air cavity and/or the large heat capacity of the structure around the corner. The relative humidity in the three rooms decreased below 30% for many days from winter to spring, probably because of the heating operation.

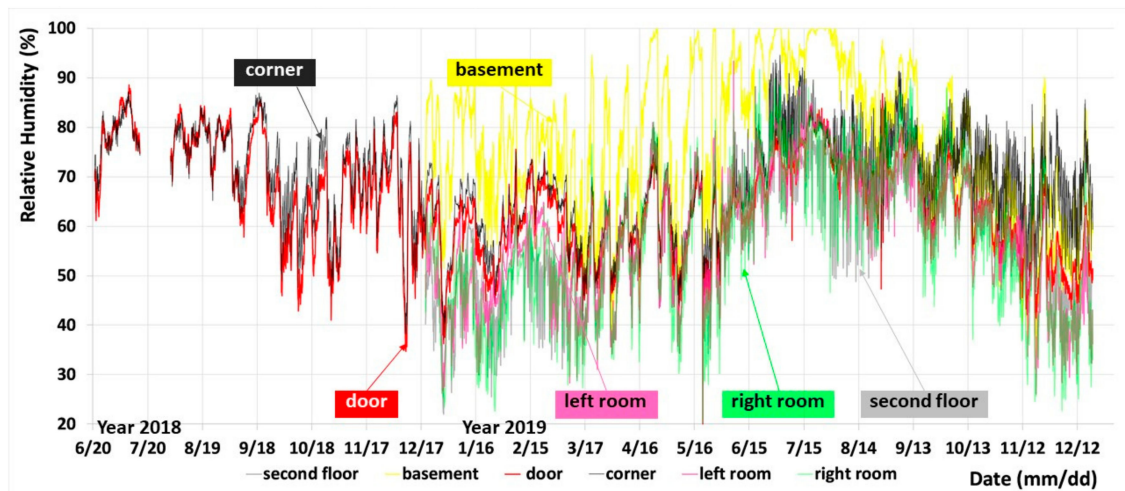


Figure 13. The measured relative humidity values of the office rooms.

4.4. Monitored Room

4.4.1. Air Temperature and Humidity

As shown in Figure 12, the air temperature near the door showed an annual change from 5 °C to 31 °C. It is lower than the outdoor temperature by approximately 5 °C and higher than that of the corner by 0.5–1 °C during daytime in summer.

Figure 13 shows that throughout the year, the monitored room was surrounded by a humid environment, that is, the outdoors and the basement. The relative humidity values of the basement and the outdoors were almost 80–90% in the night time of early summer (late June–July) and early winter (early November–December). The relative humidity near the door was also kept at high level (70–90%) from July to September, slightly lower than that of the corner.

4.4.2. Surface Temperature

Thermocouples were placed around the air cavity from June 2019 to January 2020. Their positions are shown in Figure 5 and Table 2.

Figure 14 shows the temperatures around the air cavity in the summer of 2019. The air temperature near the windowsill had a similar diurnal change with the outdoor temperature. The corner air temperature changed in parallel with that of the air in the gap between wall surface and floor board/crawl space (#3). No difference appeared between the temperatures of the wall surface (#1) and the hole surface 1 cm deep (#2). Among these temperatures, the basement and the cavity air 15 cm deep (#4) had the lowest values. The surface temperature near the air cavity (#1, #2 and #4) was lower than the dew-point temperature of outdoor air occasionally (28 and 29 June; 17, 18 and 23 July), which might have caused condensation.

Figure 15 shows the temperatures around the air cavity for several days in the summer of 2019, with the cooling operation. The air conditioner was operated in the afternoons of 26 and 27 August. The order of the temperatures is as follows:

When air conditioner was off: #3 > #W > #D > #C > #1 > #2 > 4 > #B,

while when air conditioner was on: #C > #3 > #B > #W > #1 > #2 = #4 = #D.

When the air conditioner was operated on 26 August, the temperatures significantly decreased. It is noted that when the outdoor temperature was high (at around 14:40) and the outdoor humidity was high (at around 18:40), the temperature of the cavity surface (#2) was 5.5 °C lower than the dew-point temperature of the outdoor air. Therefore, the hot air from the outdoors would have a high risk of condensation on the cold surfaces (especially for #2, the lower cavity surface) because of the cooling operation.

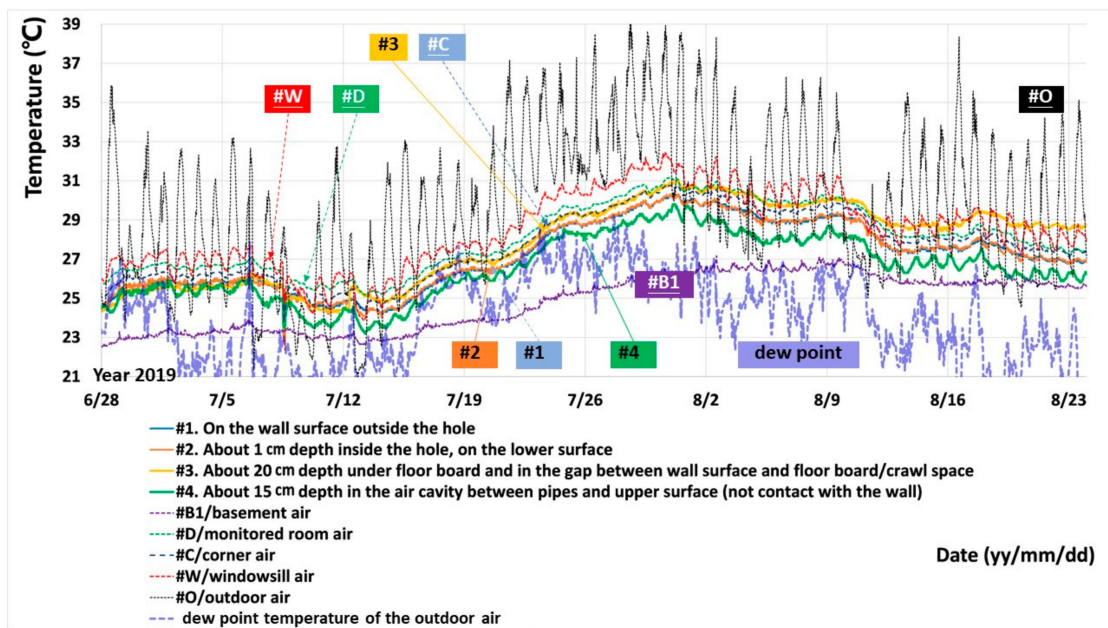


Figure 14. The temperatures around the air cavity (28 June–23 August 2019).

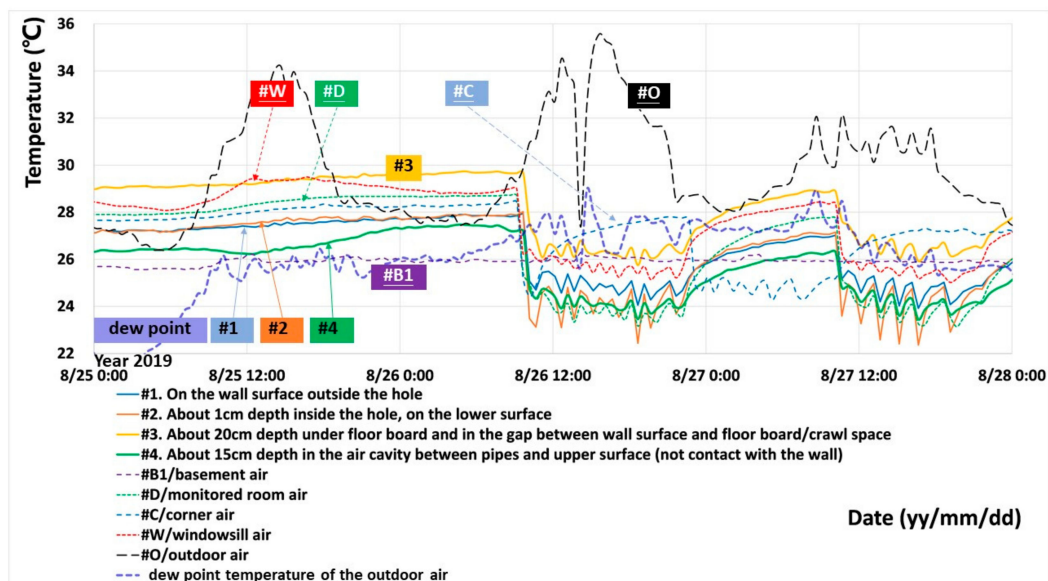


Figure 15. The temperatures around the air cavity (25–27 August 2019).

Figure 16 shows the temperatures around the air cavity in the winter of 2019/2020. The temperature of the floorboard (#11) was higher than those of the wall surface (#1) and the hole surface (#2). It might have been influenced by the crawl space made of wooden framework, in which heat was generated by electricity wires. Except for the outer part of the air cavity (#4), there seemed no risk of condensation.

4.4.3. Surface Water Content

The surface water content of the wall surface was measured on several days in the summer of 2019. Figure 6 shows the testing positions. As shown in Figure 17, compared with inner wall surfaces (C/D/E), the outer wall surfaces (A/B/F) had higher water content, especially the wall surface near the air cavity (A). The wall near door (D) and the wall near the window (A/B/F) had higher water content, so the main route for moisture transfer might be moisture adsorption to the low-temperature

wall. The moisture content of the external wall surface (M/N/P/Q/R) was much higher. On rainy days, the parts near the ground and the air cavity had more water.

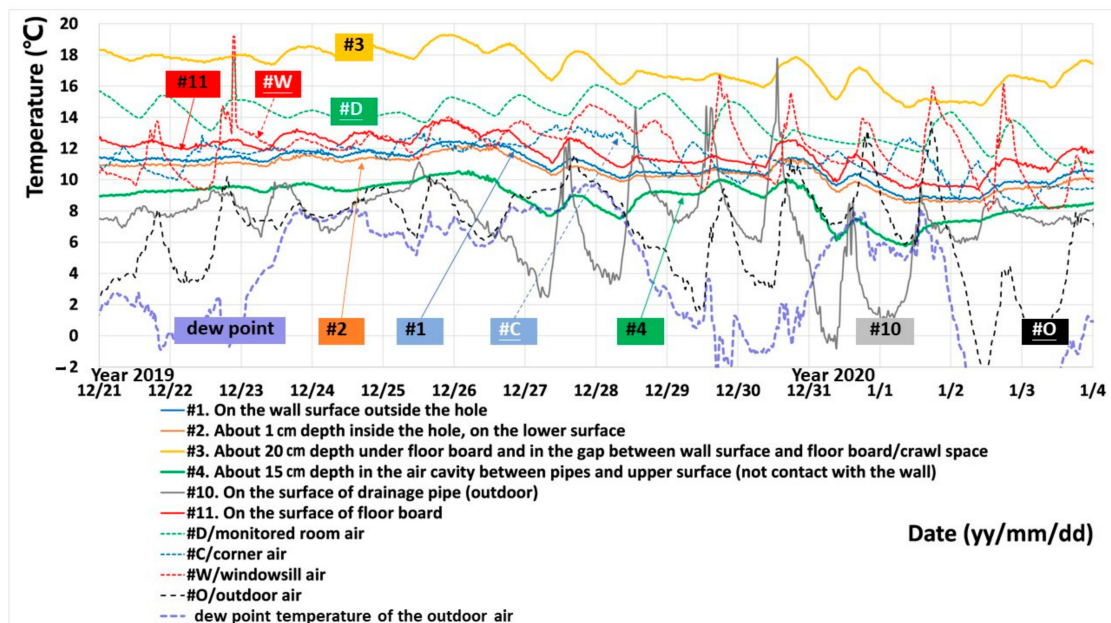


Figure 16. The temperatures around the air cavity (21 December 2019–3 January 2020).

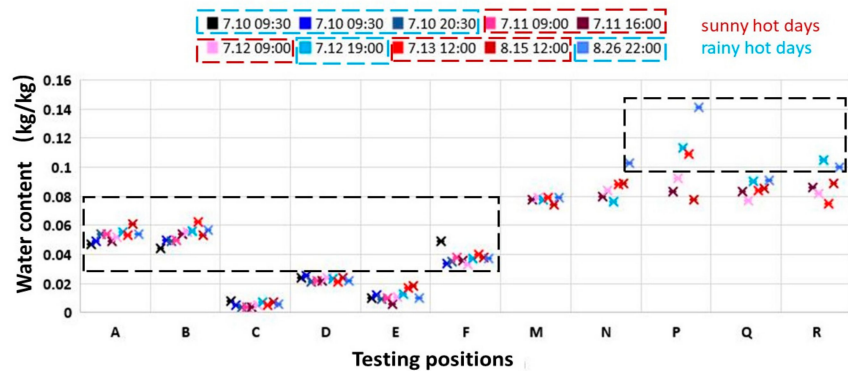


Figure 17. Water content of the measuring points.

4.5. Mold Growth Risk Analysis

Figure 18 shows the potential moisture sources. There are three periods that the absolute humidity of the monitored room (at the door) was lower than that of the outdoors/basement. From late May to early July, absolute humidity of the basement stayed higher than that of the room (at the door), while the outdoor humidity stayed higher from early June to early July and from late July to early August. The rainy season (early June–July) is indeed the risky period. Apart from wind-driven rain and rising damp, the air leakage through the air cavity provided a crucial route for moisture input.

Figure 19a shows the mold growth risk based on the air temperature and relative humidity at the door and the corner, according to Klaus Sedlbauer’s fungal spores’ germination scope evaluation. The risk at the corner was marginally higher than that at the door. Based on the ESP-r model [23], when the relative humidity and temperature combination exceeds the curve, mold growth of the matching fungi will occur. *Aspergillus penicillioides*, the commonest species in building environments, can be suitable as a crucial sensor fungus for indoor environments [47]. As shown in Figure 19b, nearly half of the figures of the air at the door and the corner, from June to September, surpass the curve of this “highly xerophilic” fungi. The corner has a rather severe scenario.

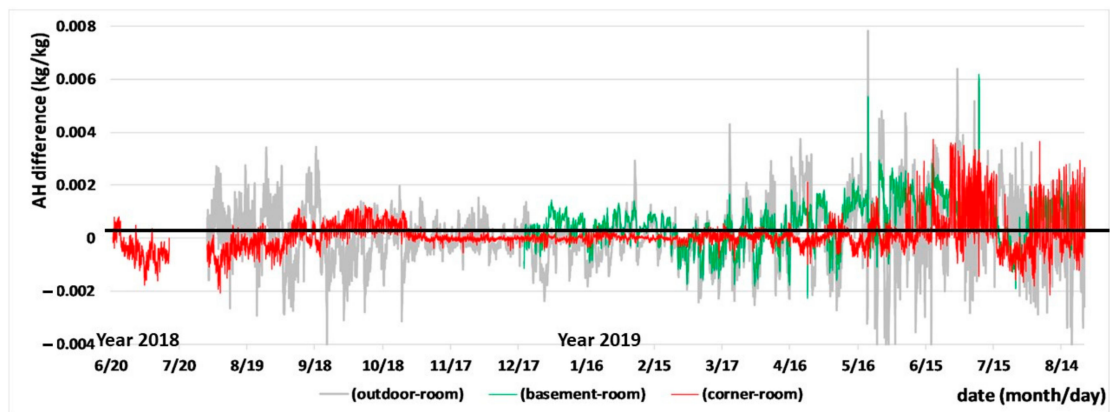


Figure 18. Absolute humidity differences between outdoor, basement, corner and room (at the door).

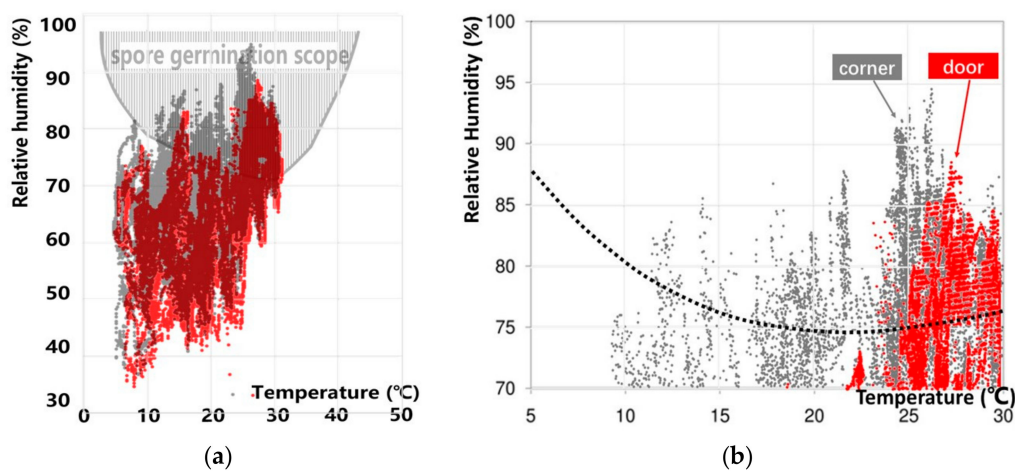


Figure 19. Mold growth risk evaluation of the indoor air at the door and the corner: (a) fungal spores' germination scope (all the months); (b) *Aspergillus penicillioides*' growth risk evaluation during summer (June–September).

5. Simulation Results and Discussion

5.1. Validation of the Proposed Hygrothermal Model

The measured data from the hygrothermometers in the monitored room (#D/door and #C/corner, near the air cavity) were used for validation purposes. As shown in Figure 20, a good agreement was obtained between the measured and calculated indoor air temperatures, and the calculated relative humidity also agrees fairly well with measured results on the whole.

Figure 21 shows the nomenclature of the cells around the air cavity: wall cells adjacent to the upper boundary cavity cells, W1–W5; the upper boundary cavity (wall surface) cells, C1–C5; air cells, A1–A5; pipe cells, P1–P5; lower boundary cavity (wall surface) cells, B1–B5. Their hygrothermal conditions and mold growth risks are compared as follows. As shown in Figure 24, a fairly good agreement can also be found between the calculated temperature of cell A1 (inner boundary of the air cavity) and the measured temperature of the cavity surface (#2).

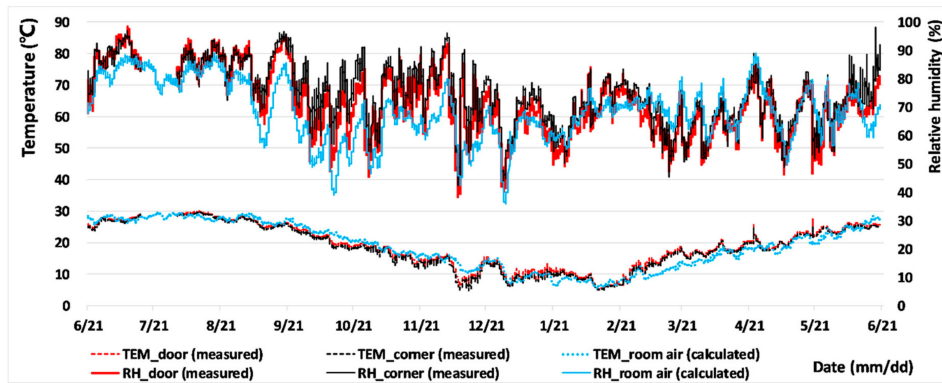


Figure 20. Comparison of the measured and calculated room temperatures and relative humidity.

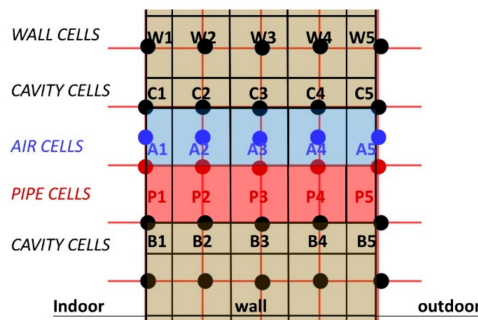


Figure 21. The nomenclature of the cells around the air cavity.

5.2. Comparison between cases with/without Air Leakage through the Air Cavity

As shown in Figure 22, air leakage through the air cavity increased the indoor absolute humidity. From June to August, the absolute humidity of the room was at a high level, regardless of whether there was air flow through the air cavity. In the following drier months (October–December), the effect of air leakage seemed to be greater, bringing more moisture to the indoors.

Figure 23 shows the calculated water content of cell C3 (on the upper surface of the cavity), in the cases with/without air leakage. Overall, the water content change of the wall surface was small throughout the year, while it remained at a higher level when the air leakage was considered. The water content in the case with air leakage reached the highest at 0.044 kg/kg from late July to early August. This agrees fairly well, although slightly lower, with the measured water content on the wall surface above the air cavity (point A, Figure 19). The difference between the water content of cell C3 in the cases with/without air leakage is 0.012 kg/kg.

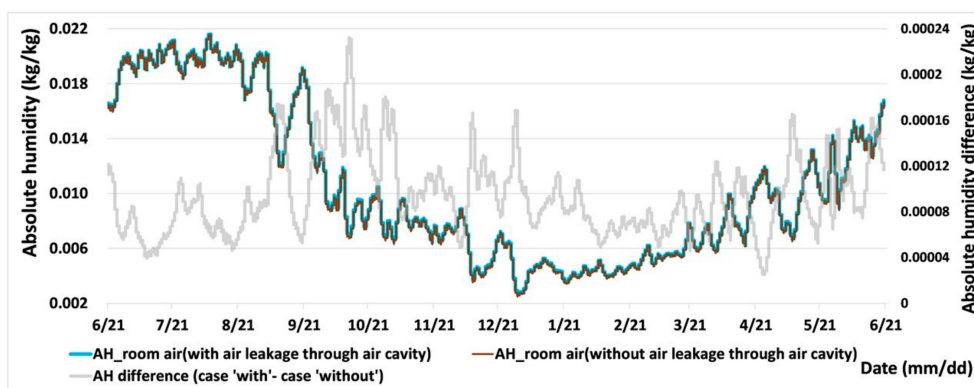


Figure 22. Calculated absolute humidity of the room air in the cases with/without air leakage through air cavity and the absolute humidity difference between both cases.

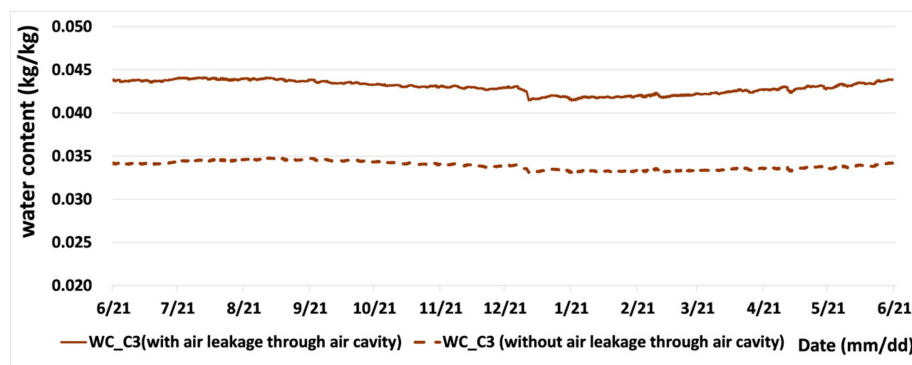


Figure 23. Calculated water content of the upper cavity cells (C3) in the cases with/without air leakage through air cavity.

5.3. Hygrothermal Conditions of the Air Cells

The calculated temperatures and relative humidity of the air cells on the interior and exterior surfaces are shown in Figure 24. The temperature and relative humidity of cell A1 shared similar fluctuations with those of the room air, while those of cell A5 had larger amplitudes, especially during winter and summer, and were probably influenced by solar radiation. Cell A1 had the potential risk of condensation and mold growth, since the relative humidity remained over 90% from late June to early September.

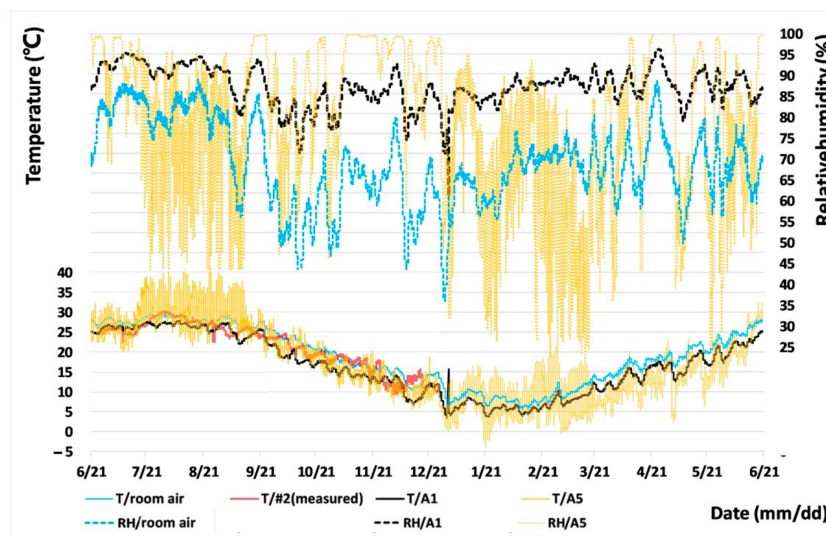


Figure 24. Calculated temperature and relative humidity of the air cells on the interior and exterior surfaces (A1 and A5).

5.4. Mold Growth Risk of Wall Cells

Figure 25a shows the mold growth risk based on the calculated temperature and relative humidity of the lower cavity cell (B3), the upper cavity cell (C3) and its upper neighboring cell (W3), according to Klaus Sedlbauer's fungal spores' germination scope evaluation. For lower cavity cell B3, nearly half of the points fall in the risky zone, which may have been influenced by the hydrophobic pipe cells. Moisture will probably accumulate and even condense on the surface between the pipe and the lower cavity boundary. For the upper cavity cell (C3) and its upper neighboring cell (W3), they also provide a suitable substrate for spores' germination, with medium risk.

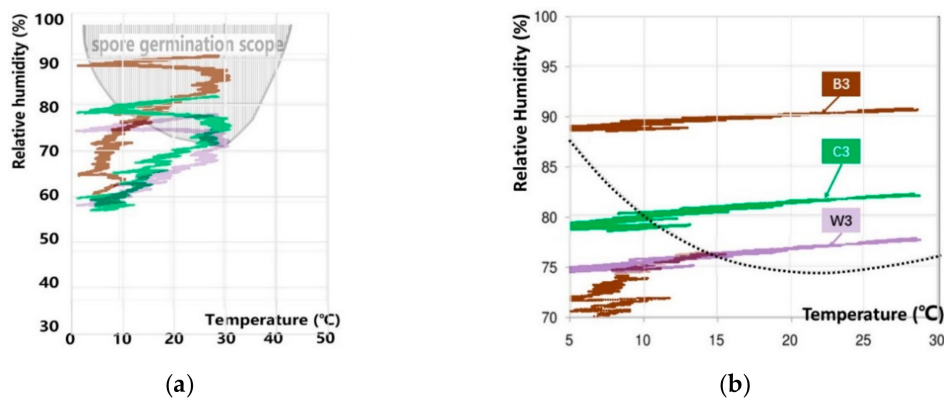


Figure 25. Mold growth risk evaluation of the wall cells (B3, C3 and W3): (a) fungal spores' germination scope (all the months); (b) *Aspergillus penicillioides*' growth risk evaluation during summer (June-September).

In Figure 25b, the *Aspergillus penicillioides* growth curve is used as an indicator. The calculated results, a temperature and relative humidity combination, of these cells from June to September, were selected. The risky proportions of all these cells exceeded 50%, especially for the upper cavity cell (C3). Sufficient hot and humid air from the outdoors might be the main reason to increase the water content on the cavity surface.

6. Conclusions

This paper investigated the effect of air leakage through the air cavity of building walls on mold growth risks. Hygrothermal measurements and a numerical simulation were implemented on a historical office building in Nanjing, China.

In this study, hygrothermal conditions were studied based on the measured datasets of hygrothermometers, thermocouples and moisture meters. The measured results and thermography data showed that the exterior wall of the monitored room was exposed to excessive moisture from the outdoors and the basement for a long period, especially during hot and rainy months, providing favorable conditions for mold growth. Three periods, from late May to early July, from early June to early July and from late July to early August, are the riskiest, during which the absolute humidity of the outdoors and the basement stays at a high level. Within diurnal change, early mornings (4–6 a.m.) and early evenings (7–9 p.m.) might be the peak time for relative humidity. It was indicated that temperature near the air cavity is obviously lower than the surrounding parts of the wall and the indoor air. As the door and window were closed, the air cavity might be the main route for air flow under the indoor and outdoor temperature and pressure differences. Therefore, it is not suitable to ventilate the room during these time periods, and dehumidification is highly required to reduce the indoor moisture.

A two-dimensional hygrothermal simulation was conducted to examine the hygrothermal conditions of the walls with air cavities penetrating the walls for air conditioner pipes, using the measured data as boundary conditions and validation. Around the air cavity, the temperature is lower, while the humidity is higher. Condensation and mold growth will occur on the cold surfaces of the cavity and the surrounding wall. The risk of fungal spores' germination and *Aspergillus penicillioides*' growth reach their peak from June to September, especially for the upper surface of the cavity. In addition, exposed to solar radiation and wind-driven rain, the outer parts of air cavity experienced an increased number of dry-wet cycles in summer.

The impacts of the air flow through the air gap between air conditioner pipes and the cavity surface on the increase in indoor humidity, water content of the cavity surface and mold growth risks were analyzed. Given that no sealing and sealing aging and shedding are frequently seen, it is of great necessity to quantify moisture-related problems regarding this phenomenon.

Moisture-related problems due to the air cavity may be tackled by controlling the building envelopes regarding moisture infiltration and exfiltration, ensuring adequate thermal insulation, sealing the cavity and controlling moisture sources. Regarding moisture sources, the ventilation time should be carefully considered as one of the room user's daily actions. The air conditioner is frequently used during working hours in summer to cool down the room, and it works to remove the indoor moisture. However, the outdoor humid air will enter the room immediately if windows are open after the users leave the offices in the early evening, during which the outdoor humidity remains at a high level throughout the day.

This paper is the first stage of the research, leaving several questions unanswered. The thermal effects of the air conditioner pipe, including the drainage pipe and intake and outlet refrigerant pipes, should be considered, and the influence of air conditioner operation remains to be evaluated. Long-term and detailed measurements, along with the validation of the proposed simulation model, should be carried out in further research.

Author Contributions: Conceptualization, Y.L. and S.H.; data curation, X.D., C.X. and Y.M.; formal analysis, X.D.; funding acquisition, Y.L.; investigation, S.H., Y.L. and X.D.; methodology, S.H. and Y.L.; project administration, Y.L.; resources, S.H., Y.L. and D.O.; software, X.D., S.H. and Y.L.; supervision, Y.L.; validation, X.D. and Y.M.; visualization, X.D. and D.O.; writing—original draft, X.D.; writing—review and editing, Y.L. and S.H. All authors have read and agreed to the published version of the manuscript.

Funding: This research was funded by National Nature Science Foundation of China (number 51878140), and the China National Key R&D Program during the 13th Five-year Plan Period (number 2019YFC1520900).

Conflicts of Interest: The authors declare no conflict of interest.

References

1. Hens, H. IEA Annex 14: Condensation and Energy. *J. Build. Phys.* **1992**, *3*, 261–273.
2. Adan, O.; Brocken, H.; Carmeliet, J. Determination of Liquid Water Transfer Properties of Porous Building Materials and Development of Numerical Assessment Methods: Introduction to the EC, HAMSTAD Project. *J. Build. Phys.* **2004**, *27*, 253–260. [[CrossRef](#)]
3. Becker, R. Condensation and Mold Growth in Dwellings—Parametric and Field Study. *Build. Environ.* **1984**, *19*, 243–250. [[CrossRef](#)]
4. World Health Organization Regional Office for Europe. *Guidelines on Indoor Air Quality: Dampness and Mold*; Druckpartner Moser: Berlin, Germany, 2009.
5. Hirota, K.; Shibuya, S.; Sakamoto, S.; Kashima, S. *A Methodology of Estimation on Air Pollution and Its Health Effects in Large Japanese Cities. Air Quality—Monitoring and Modeling*; University Library of Munich: Munich, Germany, 2012.
6. World Health Organization. *Development of WHO Guidelines for Indoor Air Quality: Dampness and Mold*; Report on a working group meeting Bonn; WHO: Bonn, Germany, 2007.
7. World Health Organization. *Indoor Air Pollutants: Exposure and Health Effects*. In *Working Group on Assessment and Monitoring of Exposure to Indoor Pollutants*; WHO: Nordlingen, Germany, 1983.
8. Sharpe, R.A.; Bearman, N.; Thornton, C.R.; Husk, K.; Osborne, N.J. Indoor fungal diversity and asthma: A meta-analysis and systematic review of risk factor. *J. Allergy Clin. Immunol.* **2015**, *135*, 110–122. [[CrossRef](#)] [[PubMed](#)]
9. Biagini, J.M.; LeMasters, G.K.; Ryan, P.H.; Levin, L.; Reponen, T.; Bernstein, D.; Villareal, M.; Khurana, H.G.K.; Burkle, J. Environmental risk factors of rhinitis in early infancy. *Pediatric Allergy Immunol.* **2010**, *17*, 278–284. [[CrossRef](#)] [[PubMed](#)]
10. Crook, B.; Burton, N.C. Indoor molds, sick building syndrome and building related illness. *Fungal Biol. Rev.* **2010**, *24*, 106–113. [[CrossRef](#)]
11. Mudarri, D.; Fisk, W.J. Public health and economic impact of dampness and mold. *Indoor Air* **2007**, *17*, 226–235. [[CrossRef](#)]
12. Lu, C.; Deng, Q.; Li, Y.; Sundell, J.; Norback, D. Outdoor air pollution, meteorological conditions and indoor factors in dwellings in relation to sick building syndrome (SBS) among adults in China. *Sci. Total Environ.* **2016**, *560–561*, 186–196. [[CrossRef](#)]

13. Adan, O. On the fungal defacement of interior finishes. Ph.D. Thesis, Technische Universiteit Eindhoven, Eindhoven, The Netherlands, 1994.
14. Becker, R.; Puterman, M. Verhütung von Schimmelbildung in Gebäuden. Teil 2: Einfluss der Oberflächenmaterialien. *Bauphysik* **1987**, *4*, 107–110.
15. Grinbergs, L.; Hyppel, A.; Hoglund, I.; Ottoson, G. *Wet-room wall systems—Mold resistance. Proceedings of the International Symposium Energy Efficient Buildings (Design, Performance and Operation) of the CIB Working Commission W67 “Energy Conservation in the Built Environment” and IEA-SHC Working Task Group XIII “Low Energy Buildings”*; IRB Verlag: Stuttgart, Germany, 1993.
16. Krieger, J.; Jacobs, D.E.; Ashley, P.E.; Baeder, A.; Chew, C.L.; Dearborn, H.; Hynes, H.P.; Miller, J.D.; Morley, R.; Rabito, F. Housing interventions and control of asthma-related indoor biologic agents: A review of the evidence. *J. Public Health Manag. Pract.* **2010**, *16*, s11–s20. [[CrossRef](#)]
17. Vereecken, E.; Roels, S. Review of mold prediction models and their influence on mold risk evaluation. *Build. Environ.* **2012**, *51*, 296–310. [[CrossRef](#)]
18. Ayerst, G. The effect of moisture and temperature on growth and spore germination in some fungi. *J. Stored Prod. Res.* **1969**, *5*, 127–141. [[CrossRef](#)]
19. Smith, S.L.; Hill, S.T. Influence of temperature and water activity on germination and growth of *Aspergillus restrictus* and *A. versicolor*. *Trans. Br. Mycol. Soc.* **1982**, *79*, 558–560. [[CrossRef](#)]
20. Sedlbauer, K.; Krus, M.; Zillig, W.; Kunzel, H.M. Mold growth prediction by computational simulation. *Journal of the Society of Materials Science Japan* **2014**, *42*, 1265–1270.
21. Clarke, J.A.; Johnstone, C.M.; Kelly, N.J.; McLean, R.C.; Anderson, J.A.; Rowan, N.J. A technique for the prediction of the conditions leading to mold growth in buildings. *Build. Environ.* **1999**, *34*, 515–521. [[CrossRef](#)]
22. Rowan, N.; Johnstone, C.; Craig, R.; Anderson, J.; Clarke, J. Prediction of toxigenic fungal growth in buildings by using a novel modelling system. *Appl. Environ. Microbiol.* **1999**, *65*, 4814–4821. [[CrossRef](#)]
23. Ojanen, T.; Peuhkuri, R.; Viitanen, H.; Lähdesmäki, K.; Vinha, J.; Salminen, K. Classification of material sensitivity: A new approach for mold growth modeling. In Proceedings of the 9th Nordic Symposium on Building Physics, Tampere, Finland, 2011; pp. 867–874.
24. Abe, K.; Nagao, Y.; Nakada, T.; Sakuma, S. Assessment of indoor climate in an apartment by use of a fungal index. *Appl. Environ. Microbiol.* **1996**, *62*, 959–963. [[CrossRef](#)]
25. Hukka, A.; Viitanen, H.A. A mathematical model of mold growth on wooden material. *Wood Sci. Technol.* **1999**, *33*, 475–485. [[CrossRef](#)]
26. Sedlbauer, K. Prediction of Mold Fungus Formation on the Surface of and Inside Building Components. Ph.D. Thesis, Universität Stuttgart, Stuttgart, Germany, 2014.
27. Guo-Jie, C.; You-Ming, C.; Xiang-Wei, L.; Xing-Guo, G. Mold germination risk evaluation inside the hygroscopic wall in south of China. *J. Saf. Environ. (in Chinese)*. **2017**, *17*, 730–734.
28. Masaru, A. Moisture Stress of Wind-Driven Rain on Building Enclosures. Ph.D. Thesis, KU Leuven, Leuven, Belgium, 2009.
29. Franzoni, E. Rising damp removal from historical masonries: A still open challenge. *Constr. Build. Mater.* **2014**, *54*, 123–136. [[CrossRef](#)]
30. Biseniece, E.; Žogla, G.; Kamenders, A.; Purviņš, R.; Kašs, K.; Vanaga, R.; Blumberga, A. Thermal performance of internally insulated historic brick building in cold climate: A long term case study. *Energy Build.* **2017**, *152*, 577–586. [[CrossRef](#)]
31. Walker, R.; Pavia, S. Thermal and moisture monitoring of an internally insulated historic brick wall. *Build. Environ.* **2018**, *133*, 178–186. [[CrossRef](#)]
32. Harrestrup, M.; Svendsen, S. Full-scale test of an old heritage multi-storey building undergoing energy retrofitting with focus on internal insulation and moisture. *Build. Environ.* **2015**, *85*, 123–133. [[CrossRef](#)]
33. Xinyuan, D.; Shuichi, H.; Yonghui, L.; Changchang, X.; Ma, Y. Evaluation of mold growth risks due to air leakage through air cavity of the building walls. In Proceedings of the MATEC Web of Conferences, Prague, Czech, 2019; Volume 282, p. 02060. [[CrossRef](#)]
34. Zhijian, L.; Shengyuan, M.; Guoqing, C.; Chong, M.; Bao-Jie, H. Distribution characteristics, growth, reproduction and transmission modes and control strategies for microbial contamination in HVAC systems: A literature review. *Energy Build.* **2018**, *177*, 77–95.
35. Zhijian, L.; Haotian, N.; Rui, R.; Guoqing, C.; Bao-Jie, H.; Qihong, D. An experiment and numerical study of resuspension of fungal spore particles from HVAC ducts. *Sci. Total Environ.* **2020**, *708*, 134742.

36. Ebbenhøj, N.E.; Meyer, H.W.; Würtz, H.; Suadicani, P.; Valbjørn, O.; Sigsgaard, T.; Gyntelberg, F. Molds in floor dust, building-related symptoms, and lung function among male and female schoolteachers. *Indoor Air* **2005**, *15*, 7–16. [[CrossRef](#)]
37. Karagiozis, H. *Impact of air leakage on the thermal and moisture performance of the building envelope*; Office of Scientific & Technical Information Technical Reports; Oak Ridge National Laboratory: Tennessee, TN, USA, 2001.
38. Synnefa, A.; Vasilakopoulou, K.; Masi, R.F.D.; Kyriakodis, G.E.; Londorfos, V.; Mastrapostoli, E.; Theoni Karlessia, T.; Santamouris, M. Transformation through renovation: An energy efficient retrofit of an apartment building in Athens. *Procedia Eng.* **2017**, *180*, 1003–1014. [[CrossRef](#)]
39. Ri, N.; Shengmao, L.; Zhigang, S.; Linxia, G. Evaluating Energy Loss through Recessed Lighting Fixtures (RLF) in Residential Buildings through a Case Study. In Proceedings of the Computing in Civil and Building Engineering, 2014 International Conference on Computing in Civil and Building Engineering, Orlando, FL, USA, 2014.
40. Gaëlle, G.; Geoffroy, H.; Ondarts, M.; Léna, M.; Woloszyn, M. Modelling the impact of multizone airleakage on ventilation performance and indoor air quality in low-energy homes. *Build. Simul.* **2019**, *2*, 1–19.
41. Coulter, J.; Davis, B.; Dastur, C.; Malkin-Weber, M.; Dixon, T. Liabilities of Vented Crawl Spaces and Their Impacts on Indoor Air Quality in Southeastern U.S. Homes. In Proceedings of the Clima 2007 Well Being Indoors (9th REHVA World Congress): the Influence of Blinds on Temperatures and Air Flows within Ventilated, Helsinki, Finland, 2007.
42. Prah, D.; Shaffer, M. *Moisture Risk in Unvented Attics Due to Air Leakage Paths*; U.S. Department of Energy: Washington, DC, USA, 2014.
43. Matsumoto, M. Simultaneous Heat and Moisture Transfer and Moisture Accumulation in Buildings. Ph.D. Thesis, Kyoto University, Kyoto, Japan, 1978.
44. Yonghui, L.; Daisuke, O.; Shuichi, H.; Takeshi, I. Effects of emergency preservation measures following excavation of mural paintings in Takamatsuzuka Tumulus. *J. Build. Phys.* **2012**, *36*, 117–139.
45. Xie, H. Analysis of performance degradation of the Chinese traditional blue bricks based on the theory of heat and moisture transfer. Master Thesis, Southeast University, Nanjing, China, 2015.
46. Shuichi, H.; Tetsuro, I.; Nitta, K. *Building Environment Engineering II: Heat, Moisture and Ventilation*; Asakura store: Tokyo, Japan, 2002; Volume 37.
47. Abe, K. Assessment of home environments with a fungal index using hydrophilic and xerophilic fungi as biologic sensors. *Indoor Air* **2012**, *22*, 173–185. [[CrossRef](#)]



© 2020 by the authors. Licensee MDPI, Basel, Switzerland. This article is an open access article distributed under the terms and conditions of the Creative Commons Attribution (CC BY) license (<http://creativecommons.org/licenses/by/4.0/>).